J. Appl. Comput. Mech., 11(2) (2025) 371-381
DOI: 10.22055/jacm.2024.46885.4616

ISSN: 2383-4536
jacm.scu.ac.ir

Shahid Chamran University of Ahvaz

Journal of Applied and Computational Mechanics

Research Paper

Electro-magnetic Enhanced Mixed-convection of a Confined Slot NEPCM-water Impinging Jet Equipped with Metal Foam

Mehdi Hashemi-Tilehnoee[1], Seyyed Masoud Seyyedi[2,3], Elena Palomo del Barrio[1,4], Farhad Hosseinnejad[5], Mohsen Sharifpur[6,7]

[1] Centre for Cooperative Research on Alternative Energies (CIC energiGUNE), Basque Research and Technology Alliance (BRTA), Alava Technology Park, Albert Einstein 48, 01510 Vitoria-Gasteiz, Spain, Email: mhashemi@cicenergigune.com

[2] Department of Mechanical Engineering, Aliabad Katoul Branch, Islamic Azad University, Aliabad Katoul, Iran

[3] Energy Research Center, Aliabad Katoul Branch, Islamic Azad University, Aliabad Katoul, Iran

[4] IKERBASQUE Basque Foundation for Science, Plaza Euskadi 5, 48009 Bilbao, Spain

[5] Department of Mechanical Engineering, Sari Branch Islamic Azad University, Sari, Iran

[6] School of Mechanical, Industrial and Aeronautical Engineering, University of the Witwatersrand, Private Bag 3, Wits 2050, South Africa

[7] Department of Medical Research, China Medical University Hospital, China Medical University, Taichung, Taiwan, Email: mohsen.sharifpur@wits.ac.za

Received May 12 2024; Revised July 29 2024; Accepted for publication July 30 2024.
Corresponding authors: M. Hashemi-Tilehnoee (mhashemi@cicenergigune.com); M. Sharifpur (mohsen.sharifpur@wits.ac.za)

Abstract. This study tackles a complicated heat transfer problem about the cooling capability of a confined slot NEPCM-water suspension impinging jet for cooling a hot surface within the mixed convective region (with $Ri = 1$ and $Re = 100$ and 300). A NEPCM-water slurry comprises nano-sized capsules containing phase change material particles dispersed in a water-based solution. The cooling medium involves a porous metal foam ($Da = 0.001$), and the entire configuration is subjected to a uniform magnetic field that satisfies the laminar region ($Ha = 50$, $\lambda = -75°$) and electric field (between the surface and confining wall). The non-dimensional governing equations of both the fluid and electromagnetic field are solved by ANSYS Fluent. This involves implementing a nondimensionalization scheme and incorporating additional partial differential equations (PDEs) into the code. Additionally, memory allocation is optimized for efficient execution. Flow patterns, isotherms, heat capacity ratio, entropy generation components, and Bejan number are computed for both water and a 2% NEPCM-water suspension. The findings indicate that increasing the Reynolds number from 100 to 300, coupled with the introduction of electromagnetic fields (EMF) enhances Nu_{ave} by 67.1% for the NEPCM-water slurry. However, this increase in heat transfer is accompanied by a proportional rise in entropy generation under EMF at $Re = 300$. Interestingly, the simultaneous application of electric and magnetic fields results in a notable reduction in entropy generation, with N_{gen} decreasing by 35% and 14% for the NEPCM-water suspension at $Re = 100$ and 300, respectively, compared to pure water. Moreover, the average Bejan number (Be_{ave}) exhibits a decreasing trend with increasing Reynolds numbers, indicating a diminishing relative importance of heat transfer irreversibility. By the introduction of EMF, Be_{ave} demonstrates a 35.9% decline for NEPCM suspension at $Da = 0.001$ as Re increases from 100 to 300. These results underscore the complex interplay among fluid dynamics, electromagnetic fields, and entropy generation in impinging jet systems, offering effective understandings for improving heat transfer methods across many industrial applications.

Keywords: EMF, Impinging jet, Ansys Fluent, NEPCM, Mixed convection, EHD.

1. Introduction

Understanding the intricate interplay between fluid dynamics and thermal management in the vicinity of magnetic fields, electric fields, or electromagnetic fields (EMF) has been a compelling pursuit for decades. In today's landscape, driven by the pressing demands for compact high-performance computing devices and the relentless pursuit of advancements in solar energy utilization, electric machinery, fuel cells, hydrogen engines, and cleaner technologies, the application of hot spot cooling techniques has emerged as a focal point of interest for both industry professionals and researchers at the forefront of scientific exploration [1]. One of the well-recognized techniques for heat removal from high thermal power density sources is known as impinging jet cooling [2]. Therefore, the possibility of the use of the electromagnetic field as a modern approach for enhancing the efficiency of the impinging jet cooling system can be more interesting in comparison with the conventional passive enhancement methods [3, 4]. Numerous researchers have conducted both numerical simulations and experimental investigations to explore the heat transfer characteristics of jet impingement while employing various methods for enhancing heat transfer, including both active and passive techniques. Extensive literature reviews on the subject of heat transfer in impinging jets are available in the

Published online: August 09 2024

references [5, 6]. In addition to traditional approaches for enhancing the efficiency of impinging jets -such as the geometrical modification of the medium and nozzle, adjusting surface roughness, exploring different flow regimes, and utilizing extended surfaces- researchers have explored innovative methods including the use of porous media, metal foam, ribs, and dimples [7-18]. Furthermore, some studies have focused on incorporating nanoparticles into base liquids to improve thermal conductivity [19-21]. Additionally, other researchers have advocated for the use of slurries containing PCM encapsulated at micro and nano scales instead of conventional nanofluids [22-27]. Mohib Ur Rehman et al. [28] demonstrated that nonliquids enhance heat transfer by increasing efficient thermal conductivity while NEPCM suspensions augment the heat removal efficiency by enhancing the capacity of the latent heat storage. Indeed, the thermal performance of fluids containing nanoparticles can be further enhanced with increased particle concentrations. Notably, NEPCM slurry outperforms nanofluids at similar particle loadings. For a thorough understanding of the use of nanoparticles and NEPCM slurry, readers are encouraged to consult the comprehensive review conducted by Mohammadpour and Lee [29]. Recently, some researchers have specifically focused on experimental research aimed at enhancing impinging jet heat transfer techniques using metal foams filled with solid-liquid phase change materials [30, 31]. In parallel, researchers have initiated the utilization of magnetic fields in impingement jet cooling systems [1, 32-35]. The utilization of a magnetic field allows for the manipulation of fluid flow, the induction of stirring or mixing, and the modification of heat transfer characteristics. This methodology finds common application in the field of magnetohydrodynamics (MHD), which explores the interaction between magnetic fields and electrically conductive fluids. The objective is to actively control or enhance heat transfer by leveraging the magnetic field [36-38]. In 2023, Selimefendigil and Öztop [39] numerically evaluated the performance of a system of multiple impinging jets including an encapsulated phase change material in the form of a packed bed under the control of magnetic fields. The findings revealed that the spatial average Nusselt number significantly increased when employing PCM in the impinging jet system and nanoliquid, particularly at the highest Hartmann number. From existing literature, it is evident that traditional methods effectively enhance heat transfer, while the addition of nanoparticles and the use of encapsulated phase change materials (PCMs) significantly improve cooling performance in impingement systems. However, the introduction of a magnetic field, while serving to control fluid flow, inherently decreases cooling performance. In this study, we aim to investigate a confined slot-impinging jet subjected to both magnetic and electric fields. Notably, the magnetic field will be applied in a direction aimed at increasing heat transfer. The jet fluid consists of a mixture of water and NEPCM suspension, with flow occurring through a porous medium known as metal foam in the mixed convection region. The novelty of this study stands out compared to previous works by focusing on the positive impact of magnetic fields to improve the performance of the impinging jet system. We successfully applied the complex equations of the electric field to the cooling system of the impingement jet, analyzing the thermal management problem and adherence to the 2nd thermodynamics law. Furthermore, we explore the effects of using metal foam and NEPCM suspension to enhance heat transfer. Finally, from a numerical standpoint, we convert the system of complicated equations into non-dimensional form equations and solve them using the Ansys-Fluent finite volume CFD code, with careful consideration of user-defined -scalars and -functions.

2. Problem Statement and Formulation

Figure 1 schematically illustrates a wall-confined single-slot impingement jet heat removal system. The bottom surface or impinging surface is kept at T_h fixed temperature. Positioned above is the upper confiner wall, which is thermally and electrically insulated and features a central slot. A uniform cooling jet impacts the hot wall at a perpendicular angle, with the U_{in} jet inlet velocity and temperature of T_c. The inlet jet passes downward through a porous medium made of metal foam. The slot is presumed to a sufficient extent to induce a two-dimensional planar jet flow, a configuration commonly observed in literature. This design choice results in a superior impingement region and guarantees consistent cooling distribution post-impinging. Notably, a big aspect ratio is defined to maximize heat transfer [1, 40]. To minimize computational expenses half of the model, which meets symmetrical conditions, is modeled. The slot hydraulic diameter, denoted as D_h, serves as the origin for nondimensionalizing all geometric lengths. The working fluid is a 2% suspension of the NEPCM water. A no-slip condition is imposed on all surfaces. The vector of the applied uniform magnetic field is directed to assist the forces in the medium for enhancing the heat transfer. Uniform electric potentials of ϕ_0 and ϕ_1 where $\phi_0 < \phi_1$ applied to the uppers and lower walls act as collector and emitter, respectively to accomplish an electric field. As a result, the uniform electric charge density along with the charge carrier mobility, represented by K, is introduced into the fluid medium through the bottom wall.

2.1. Numerical equations

The flow condition is supposed to be steady-state, incompressible, and two-dimensional with constant fluid constraints to analyze the mixed convection flow. The effects of viscous dissipation and radiation are disregarded. Maxwell's equations for electromagnetic fields, fluid conservation equations that utilize the Boussinesq approximation, and Gauss law are employed to develop the governing equations of the system. Given that the problem occurs in the mixed convection region (low Reynolds numbers), modeling the porous media requires only the Darcy term, without considering the Forchheimer term [41]. Thus, under Darcy's law, a source term was added to the momentum equation for defining metal foam. So, the system of equations of NEPCM-water suspension is as follows [4, 42-44]:

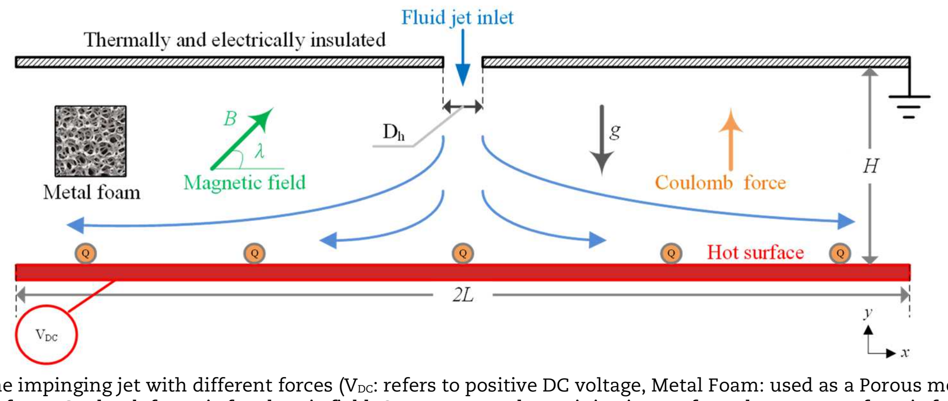

Fig. 1. Schematic of the impinging jet with different forces (V_{DC}: refers to positive DC voltage, Metal Foam: used as a Porous medium, Magnetic field: is for applying Lorentz force, Coulomb force: is for electric field, Q: represents charge injection surface, the upper surface: is for negative DC voltage).

$$\frac{\partial u}{\partial x}+\frac{\partial v}{\partial y}=0 \tag{1}$$

$$u\frac{\partial u}{\partial x}+v\frac{\partial u}{\partial y}=-\frac{1}{\rho_b}\frac{\partial p}{\partial x}+\left(\frac{\partial^2 u}{\partial x^2}+\frac{\partial^2 u}{\partial y^2}\right)\nu_b+\frac{qE_{0x}}{\rho_b}+(v\sin\lambda\cos\lambda-u\sin^2\lambda)\frac{\sigma_b B_0^2}{\rho_b}-\frac{\nu_b}{\kappa}u \tag{2}$$

$$u\frac{\partial v}{\partial x}+v\frac{\partial v}{\partial y}=-\frac{1}{\rho_b}\frac{\partial p}{\partial y}+\left(\frac{\partial^2 v}{\partial x^2}+\frac{\partial^2 v}{\partial y^2}\right)\nu_b+g\beta_b(T-T_c)+\frac{qE_{0y}}{\rho_b}+\left(u\sin\lambda\cos\lambda-v\cos^2\lambda\right)\frac{\sigma_b B_0^2}{\rho_b}-\frac{\nu_b}{\kappa}v \tag{3}$$

$$u\frac{\partial T}{\partial x}+v\frac{\partial T}{\partial y}=\left(\frac{\partial^2 T}{\partial x^2}+\frac{\partial^2 T}{\partial y^2}\right)\frac{k_b}{(\rho C_p)_b}+\frac{1}{(\rho C_p)_b}\left(Kq\vec{E}_0-D\nabla q+q\vec{V}\right)\vec{E}_0 \tag{4}$$

$$\vec{E}_0=-\nabla\phi \tag{5}$$

$$\nabla\cdot\vec{E}_0=\frac{q}{\varepsilon} \tag{6}$$

$$\nabla\cdot(Kq\vec{E}_0-D\nabla q+q\vec{V})=0 \tag{7}$$

Bulk properties of the NEPCM-water suspension (denoted by subscript *b*) are determined by the properties of the base fluid (subscript *f*) with the NEPCM (denoted by *p*) through the following expression [43, 44]:

$$\rho_b=\rho_p\phi+\rho_f(1-\phi) \tag{8}$$

$$\left(C_p\right)_b=\frac{\phi(\rho C_p)_p+(1-\phi)(\rho C_p)_f}{\rho_b} \tag{9}$$

$$\beta_b=\beta_p\phi+\beta_f(1-\phi) \tag{10}$$

$$C_{p,p}=C_{p,co}+\frac{\pi}{2}\left(\frac{h_{sf}}{T_{Mr}}-C_{p,co}\right)\sin\left(\frac{\pi(T-T_0)}{T_{Mr}}\right)\begin{cases}0 & \text{if } T<T_{fu}-\dfrac{T_{Mr}}{2}\\ 1 & \text{if } T_{fu}-\dfrac{T_{Mr}}{2}\le T\le T_{fu}+\dfrac{T_{Mr}}{2}\\ 0 & \text{if } T>T_{fu}+\dfrac{T_{Mr}}{2}\end{cases} \tag{11}$$

$$\frac{k_b}{k_f}=N_k\phi+1 \tag{12}$$

$$\frac{\mu_b}{\mu_f}=N_\nu\phi+1 \tag{13}$$

Equations (1)-(7) convert to nondimensional equations by subsequent dimensionless definitions:

$$\begin{gathered}X=\frac{x}{D_h},Y=\frac{y}{D_h},\theta=\frac{T-T_c}{T_h-T_c},U=\frac{u}{U_{in}},V=\frac{v}{U_{in}},P=\frac{p}{\rho_b U_{in}^2},\theta_f=\frac{T_{fu}-T_c}{T_h-T_c},\\ \delta=\frac{T_{Mr}}{T_h-T_c},Q=\frac{q}{q_0},\Phi=\frac{\phi-\phi_0}{\phi_1-\phi_0},E=\frac{E_0 H}{\phi_1-\phi_0},\chi=\frac{(C_{p,co}+\iota C_{p,sh})\rho_{co}\rho_{sh}}{(\rho C_p)_f(\rho_{sh}+\iota\rho_{co})},\\ Da=\frac{\kappa}{D_h^2},D_e=\frac{\nu_b}{D},Pr=\frac{\nu_b}{\alpha_b},Ha=D_h B_0\left(\frac{\sigma_b}{\nu_b\rho_b}\right)^{0.5},Gr=\frac{g\beta_b D_h^3(T_h-T_c)}{\nu_b},\\ Re=\frac{U_{in}D_h}{\nu_b},Ri=\frac{Gr}{Re^2},E_c=\frac{\alpha_b^2}{D_h^2 C_p(T_h-T_c)},Pr_E=\frac{\nu_b}{(\phi_1-\phi_0)K},S_E=\frac{(\phi_1-\phi_0)q_0}{\rho_b U_{in}^2},N_E=\frac{D_h^2 q_0}{(\phi_1-\phi_0)\varepsilon}.\end{gathered} \tag{14}$$

leading to:

$$\frac{\partial U}{\partial X}+\frac{\partial V}{\partial Y}=0 \tag{15}$$

$$U\frac{\partial U}{\partial X}+V\frac{\partial U}{\partial Y}=-\frac{\partial P}{\partial X}+\left(\frac{\partial^2 U}{\partial X^2}+\frac{\partial^2 U}{\partial Y^2}\right)\frac{1}{Re}+S_E QE_X+\left(V\sin\lambda\cos\lambda-U\sin^2\lambda\right)\frac{Ha^2}{Re}-\frac{U}{ReDa} \tag{16}$$

$$U\frac{\partial V}{\partial X}+V\frac{\partial V}{\partial Y}=-\frac{\partial P}{\partial Y}+\left(\frac{\partial^2 V}{\partial X^2}+\frac{\partial^2 V}{\partial Y^2}\right)\frac{1}{Re}+\theta\frac{Gr}{Re^2}+S_E QE_Y+\left(U\sin\lambda\cos\lambda-V\cos^2\lambda\right)\frac{Ha^2}{Re}-\frac{V}{ReDa} \tag{17}$$

$$U\frac{\partial \theta}{\partial X}+V\frac{\partial \theta}{\partial Y}=\left(\frac{\partial^2 \theta}{\partial X^2}+\frac{\partial^2 \theta}{\partial Y^2}\right)\frac{1}{Re\,Pr}+S_E E_c\left(\frac{Q}{Re\,Pr_E}(E_X^2+E_Y^2)-\frac{1}{ReD_e}(E_X\frac{\partial Q}{\partial X}+E_Y\frac{\partial Q}{\partial Y})+Q(E_X U+E_Y V)\right) \tag{18}$$

$$\frac{\partial^2 \Phi}{\partial X^2}+\frac{\partial^2 \Phi}{\partial Y^2}=-QN_E \tag{19}$$

$$U\frac{\partial Q}{\partial X}+V\frac{\partial Q}{\partial Y}=\left(\frac{\partial^2 Q}{\partial X^2}+\frac{\partial^2 Q}{\partial Y^2}\right)\frac{1}{D_e Re}-\frac{1}{RePr_E}\left(Q\left(\frac{\partial E_X}{\partial X}+\frac{\partial E_Y}{\partial Y}\right)+E_X\frac{\partial Q}{\partial X}+E_Y\frac{\partial Q}{\partial Y}\right) \tag{20}$$

$$C_r=\frac{\rho_b C_{p,b}}{\rho_f C_{p,f}}=\phi\chi+(1-\phi)+\frac{\phi}{\delta Ste}\left\{\frac{\pi}{2}\sin\left(\frac{\pi}{\delta}\left(\theta-\theta_{fu}+\frac{\delta}{2}\right)\right)\right\}\begin{cases}0 & \text{if } \theta<\theta_{fu}-\frac{\delta}{2}\\ 1 & \text{if } \theta_{fu}-\frac{\delta}{2}<\theta<\theta_{fu}+\frac{\delta}{2}\\ 0 & \text{if } \theta>\theta_{fu}+\frac{\delta}{2}\end{cases} \tag{21}$$

The boundary conditions for the simulation domain are:

$$\begin{gathered}\theta=\frac{\partial P}{\partial n}=\frac{\partial \Phi}{\partial n}=\frac{\partial Q}{\partial n}=U=0,\ V=1 \text{ normal to inlet,}\\ \frac{\partial \theta}{\partial n}=\frac{\partial Q}{\partial n}=\Phi=U=V=0 \text{ on upper wall,}\\ \frac{\partial \theta}{\partial n}=U=\frac{\partial V}{\partial n}=\frac{\partial P}{\partial n}=0 \text{ on symmetrical wall,}\\ \theta=1,\ U=V=0,\ \Phi=1,\ Q=1 \text{ on heated surface,}\\ \frac{\partial \theta}{\partial n}=\frac{\partial U}{\partial n}=\frac{\partial V}{\partial n}=P=0 \text{ normal to outlet}\end{gathered} \tag{22}$$

The subsequent equations used to calculate Nusselt numbers on the heated surface:

$$Nu_{loc}=-\left.\frac{\partial \theta}{\partial n}\right|_{\text{hot surface}} \tag{23}$$

$$Nu_{ave}=\frac{1}{S}\int_0^S Nu_{loc}\,dS=-\frac{1}{L_x}\int\frac{\partial \theta}{\partial Y}dX \tag{24}$$

2.2. Bejan number and Entropy generation

Exergy, in accordance with the 2nd thermodynamics law, signifies the maximum work obtainable from a stream of energy or matter, while entropy indicates the dissipation of exergy. It is crucial to recognize that the primary cause of an inefficient system lies in the entropy generation or the dissipation of exergy. The rate of generated entropy is mathematically expressed by [43, 44]:

$$\dot{S}_{gen}=\left[\left(\frac{\partial T}{\partial x}\right)^2+\left(\frac{\partial T}{\partial y}\right)^2\right]k_b/T_0^2+\left[2\left(\frac{\partial u}{\partial x}\right)^2+2\left(\frac{\partial v}{\partial y}\right)^2+\left(\frac{\partial u}{\partial y}+\frac{\partial v}{\partial x}\right)^2\right]\mu_b/T_0+\frac{(E_{0X}{}^2+E_{0Y}{}^2)Kq}{T_0}+\frac{\sigma_b\left(uB_0\sin\lambda-vB_0\cos\lambda\right)^2}{T_0}+\left(u^2+v^2\right)\frac{\mu_b}{\kappa T_0} \tag{25}$$

Local entropy generation in Eq. (25) comprises five terms that correspond to entropy generation from heat transfer, viscous dissipation, electric field, magnetic field, and porous media. The dimensionless form of the locally generated entropy equation would be expressed by:

$$\begin{aligned}N_{L,gen}=\frac{\dot{S}_{gen}}{\left(\frac{\Delta T}{D_h}\right)^2\left(\frac{k_f}{T_0^2}\right)}&=\left[\left(\frac{\partial \theta}{\partial X}\right)^2+\left(\frac{\partial \theta}{\partial Y}\right)^2\right]k_b/k_f+\left[2\left(\frac{\partial U}{\partial X}\right)^2+2\left(\frac{\partial V}{\partial Y}\right)^2+\left(\frac{\partial U}{\partial Y}+\frac{\partial V}{\partial X}\right)^2\right]\frac{\mu_b}{\mu_f}\Phi_f\\ &+\left[\left(\frac{\partial \Phi}{\partial X}\right)^2+\left(\frac{\partial \Phi}{\partial Y}\right)^2\right]S_E Q\Phi_f/Pr_E+\frac{\sigma_b}{\sigma_f}Ha^2\Phi_f\left(U\sin\lambda-V\cos\lambda\right)^2+\left(U^2+V^2\right)\frac{\mu_b\Phi_f}{\mu_f Da}\end{aligned} \tag{26}$$

$$\Phi_f=\left(\frac{U_{in}}{\Delta T}\right)^2\frac{T_0\mu_f}{k_f} \tag{27}$$

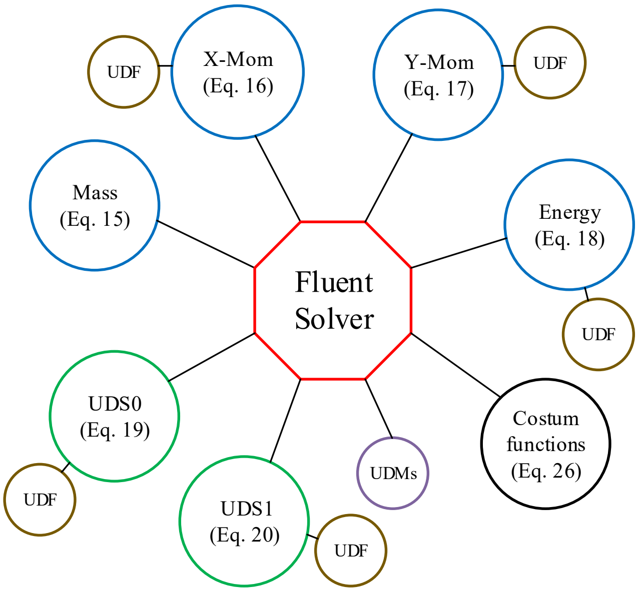

Fig. 2. The structural graph of Ansys Fluent solver for tackling the problem.

The elements of the overall generated entropy, denoted as N_{gen}, can be calculated by volumetric integrating of Eq. (26):

$$N_{gen} = \sum \int_V N_{L,mm} dV, mm = HT, FF, EF, MF, PM \tag{28}$$

The mean Bejan number utilized to quantify the irreversibility resulting from heat transfer across the whole enclosure:

$$Be_{ave} = \frac{\int_A Be_{loc} dA}{\int_A dA}, \quad Be_{loc} = \frac{N_{(L,HT)}}{N_{gen}} \tag{29}$$

3. Modeling Procedure

In this study, the pressure-based FVM method in Ansys Fluent is used to discretize the governing equations. Temperature differences in fluid characteristics are ignored when using the Boussinesq approximation for the buoyancy factor. The upper confined wall and the heated wall are considered smooth. The PISO technique is used for coupling velocity and pressure, pressure is discretized using the PRESTO scheme, and the second-order upwind scheme is used for convection contribution to the coefficients. Conservation equations have a convergence requirement of 10^{-6}. Figure 2 outlines the methods used by ANSYS Fluent to address this problem.

The electric effect is incorporated into the model through the charge density equation and the potential equation, treated as double UDS with dedicated UDFs to handle the equation's source term. Similarly, the magnetic field and the impact of porous media are included in the momentum equations through UDFs. Custom functions are employed to compute entropy generation and the Bejan number, encompassing all five terms as specified in Eq. (26). Additionally, user-defined memory is utilized to share parameters between scalars and their corresponding functions.

3.1. Meshing verification

To determine the suitable cavity mesh, a mesh sensitivity study for the water-impinging jet was undertaken, taking into account the effect of an electric field at Da = 0.001, Re = 300, Ri = 1, and AR = 10. As can be seen from Fig. 3, a grid of 100000 elements is considered ideal for producing a mesh-nondependent problem and reducing discretization uncertainty.

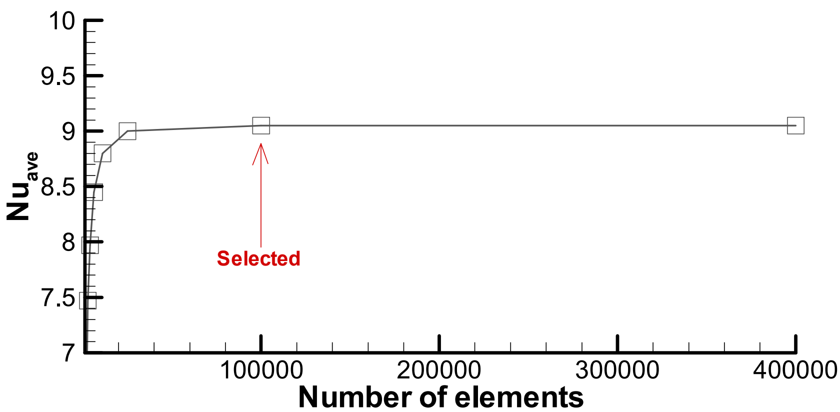

Fig. 3. Convergence of the Nu_{ave} at the heated wall.

3.2. Validation

For a slot-impinging jet domain at Re = 100, AR = 10, Re = 300, Ri = 1, and Ha = 0, we compare the findings of our modeling with the work of Sahoo and Sharif [40] to validate the computational process. The isotherms and streamlines show good overall agreement, as shown in Fig. 4, with a maximum difference of less than 1% and 5% for Re = 100 and Re = 300, respectively.

4. Results and Discussion

By applying a uniformly positive effect magnetic field and electric field, the current study examines the fluid flow, heat transfer, and entropy for the NEPCM-water jet impingement specified in section 2 utilizing water and NEPCM (2%)–water suspension. Utilizing a non-dimensionalization approach, ANSYS Fluent is employed for modeling. Polymethyl methacrylate (PMMA) makes up the NEPCM particles' shell, while n-octadecane makes up the core. We assume constants for ionic mobility and dielectric permittivity for the sake of simplicity. The buoyancy force, Coulomb force, and Lorentz force are the three main factors influencing fluid flow. With Reynolds numbers 100 and 300, the Coulomb force is fixed between the upper and bottom confinement walls. Calculations are performed for λ = -75°, Ha = 0 and 50, Re = 100, 300, Da = 0, 0.001 and Ri = 1. The jets of downward direction are chosen as the case study due to their higher efficiency compared to upward jets [40]. The anticipated ratio for the distribution of irreversibility was $\Phi_f = 10^{-4}$. According to the symmetrical considerations, the size of the jet is 0.5D_h. The parameters of the NEPCM-water slurry and other non-dimensional parameters used are illustrated in Table 1.

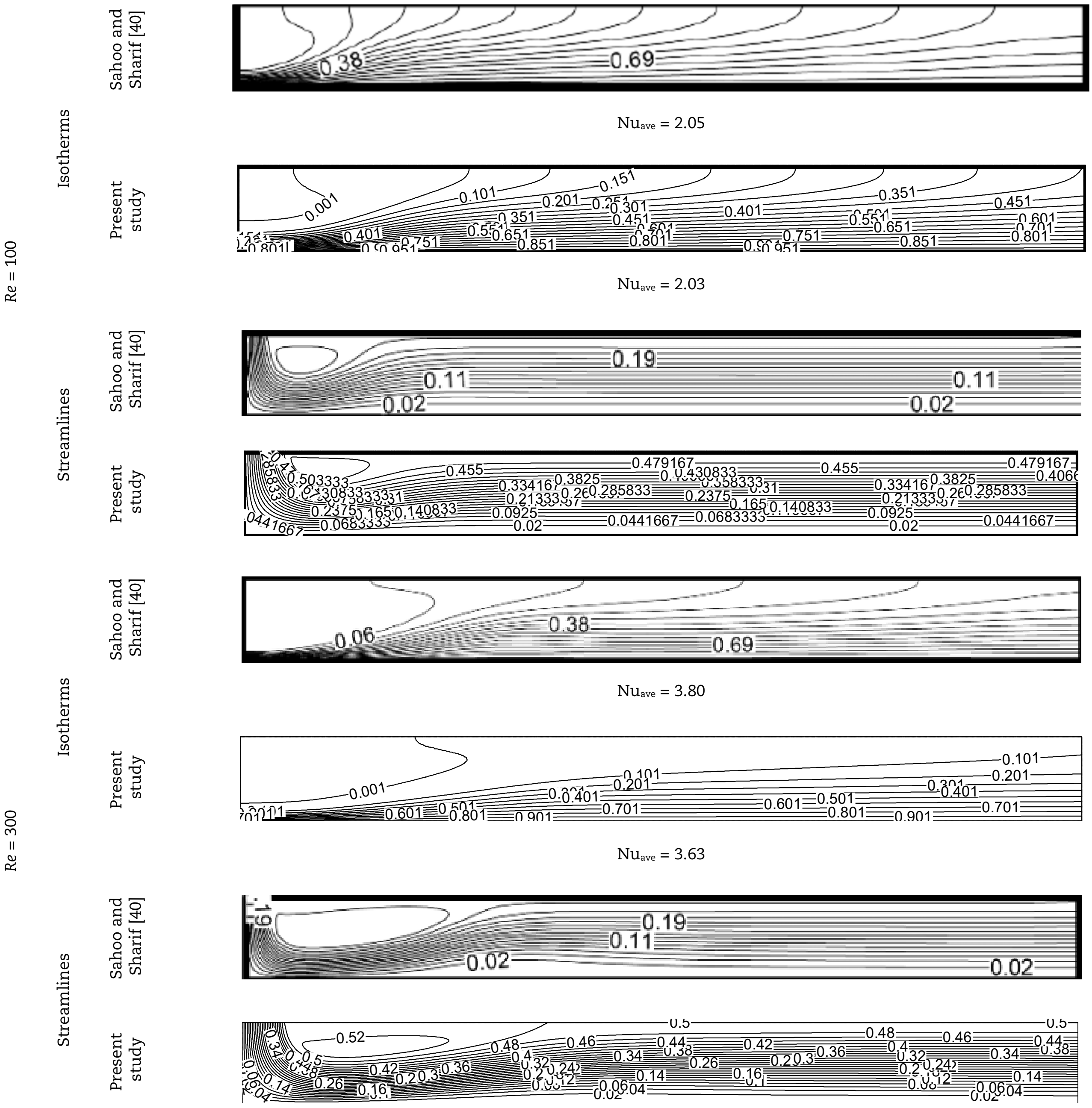

Fig. 4. Comparing the streamlines and isotherms of the present study and Ref. [40].

Table 1. The dimensionless parameters used in the calculation.

Pr_f	θ_{fu}	Pr_E	ϕ	σ	Φ	N_E	Ste	N_k	N_υ	ρ_p / ρ_f	D_E	δ	E_C	$\phi \times \beta_p / \beta_f$	S_E
6.2	0.5	1	0.02	0.4	10^{-4}	1	0.2	3	6	0.9	1	0.05	1	0	1

Table 2. The results of the stated problem modeling.

		Da = 0						*Da* = 0.001					
		Re = 100			*Re* = 300			*Re* = 100			*Re* = 300		
		WF*	EF**	EMF***	WF	EF	EMF	WF	EF	EMF	WF	EF	EMF
Water	Nu_{ave}	4.64	4.95	5.51	7.22	7.77	9.20	5.54	5.68	5.81	8.94	9.02	9.55
	Ψ_{max}	0.51	0.53	0.50	0.53	0.55	0.51	0.50	0.50	0.50	0.50	0.50	0.50
	N_{gen}	3.61	3.96	4.19	5.65	6.26	6.99	4.08	4.22	4.31	6.64	6.74	7.09
	Be_{ave}	0.58	0.69	0.66	0.41	0.54	0.50	0.41	0.40	0.40	0.26	0.26	0.25
NEPCM-suspension	Nu_{ave}	4.84	5.19	5.83	7.50	8.13	9.74	5.89	6.02	6.16	9.47	9.54	10.13
	Ψ_{max}	0.51	0.53	0.50	0.53	0.55	0.51	0.49	0.49	0.49	0.50	0.50	0.49
	N_{gen}	3.68	4.03	4.31	5.72	6.34	7.18	6.84	6.94	4.47	8.50	8.59	7.32
	Be_{ave}	0.58	0.69	0.66	0.42	0.54	0.51	0.41	0.39	0.39	0.26	0.26	0.25

* WF (Without field), ** EF (Electric field), *** EMF (Electro-Magnetic field)

The findings are showcased through Nu, streamlines, isotherms, *Be*, and *Cr* for the jet impingement of NEPCM-water suspension under normal conditions and with magnetic-electric fields. Table 2 provides a comprehensive overview of the Nu_{ave}, maximum stream function, and average Bejan number for Darcy numbers 0 and 0.001, and Reynolds numbers 100 and 300, considering both water and NEPCM-water with and without the effects of electromagnetic fields.

Table 2 shows that the Nu_{ave}, maximum stream function, and N_{gen} increase with *Re* for all cases. It is evident that increasing *Re* from 100 to 300 leads to a significant rise in Nu. For instance, in the presence of an electromagnetic field, the Nu_{ave} increases from 5.51 to 9.20 (a 67% increase) for pure water at *Da* = 0 when *Re* goes up from 100 to 300. Similarly, for NEPCM-suspension, the values of Nu_{ave} change from 5.83 to 9.74 (a 67.1% increase) at *Da* = 0. This can be attributed to the fact that the velocity of flow is proportional to the Reynolds number, as indicated by Eq. (14). As the flow velocity increases, the depth of penetration also increases. In other words, the power of flow for penetration into the metal foam increases with the velocity of flow (or Reynolds number). Consequently, according to Eqs. (16)-(18), the temperature gradient increases, and ultimately, according to Eq. (24), the Nu_{ave} enhances. The power of the flow rises with the Reynolds number as evidenced by $|\Psi_{max}|$. For example, $|\Psi_{max}|$ increases from 0.53 to 0.55 (a 3.8% increase) for pure water at *Da* = 0 when *Re* goes up from 100 to 300 in the presence of EF. Although the Nu_{ave} increases with increasing *Re*, it also leads to an increase in the N_{gen}. For EMF, the values of N_{gen} increases from 4.19 to 6.99 (a 66.8% increase) for pure water at *Da* = 0 when *Re* goes up from 100 to 300. Similarly, for NEPCM-suspension, the values of N_{gen} change from 4.31 to 7.18 (a 66.6% increase) at *Da* = 0. The reason for this increase is clear. When the temperature gradient increases, the entropy generation number goes up, as indicated by Eq. (26). It is important to note that, as defined by the Darcy number, it correlates directly with the permeability of a porous medium, which in turn defines the intensity of flow inside the medium. For water in a medium without metal foam, the Nusselt number increased by 55%, and in a medium filled by metal foam, it increased by 61% where entropy generation increased by 55% and 60%, respectively. However, the best results for entropy generation are observed with the NEPCM-water suspension. By increasing the *Re* to 300, N_{gen} increases to 24.26% without fields and 23.77% with electromagnetic fields. The table also demonstrates that the values of the Nu_{ave} ascend in the presence of EF or EMF compared to without a field (WF). For example, the values of mean Nu are 8.94, 9.02 and 9.55 for pure water at *Da* = 0.001 and *Re* = 300, for WF, EF, and EMF respectively. Similarly, these values are 9.47, 9.54, and 10.13 for NEPCM-suspension, confirming this trend. In the presence of a magnetic field, the movement of a conductive fluid generates electric currents. The interaction between these currents and the magnetic field produces the Lorentz force, which can alter the flow pattern of the fluid. This force can create secondary flows or enhance turbulence, leading to increased mixing and more effective heat transfer. On the other side the Coulomb force because the electric field is also in the direction of the buoyancy force leads to the formation of secondary flows or enhanced mixing in the fluid. Therefore, according to the results in the case of the fluid conjugated with metal foam, the impacts of the magnetic and electric fields have a better effect in a medium that is free of porosity. The magnetic field in this study was targeted at such a proper angle that it synergized with other forces in the fluid region, thereby increasing heat transfer capability. The impact of the electric field at *Re* = 300 was very low in metal foam however, when it combined with the magnetic vector, the Nu increased significantly. For example, in the case of NEPCM water suspension, the Nusselt number increased by about 1%, but when the magnetic field supplemented the electric field, the Nusselt number increased to about 7%. Moreover, simultaneously using the electric and magnetic fields leads to a significant decrease in entropy generation.

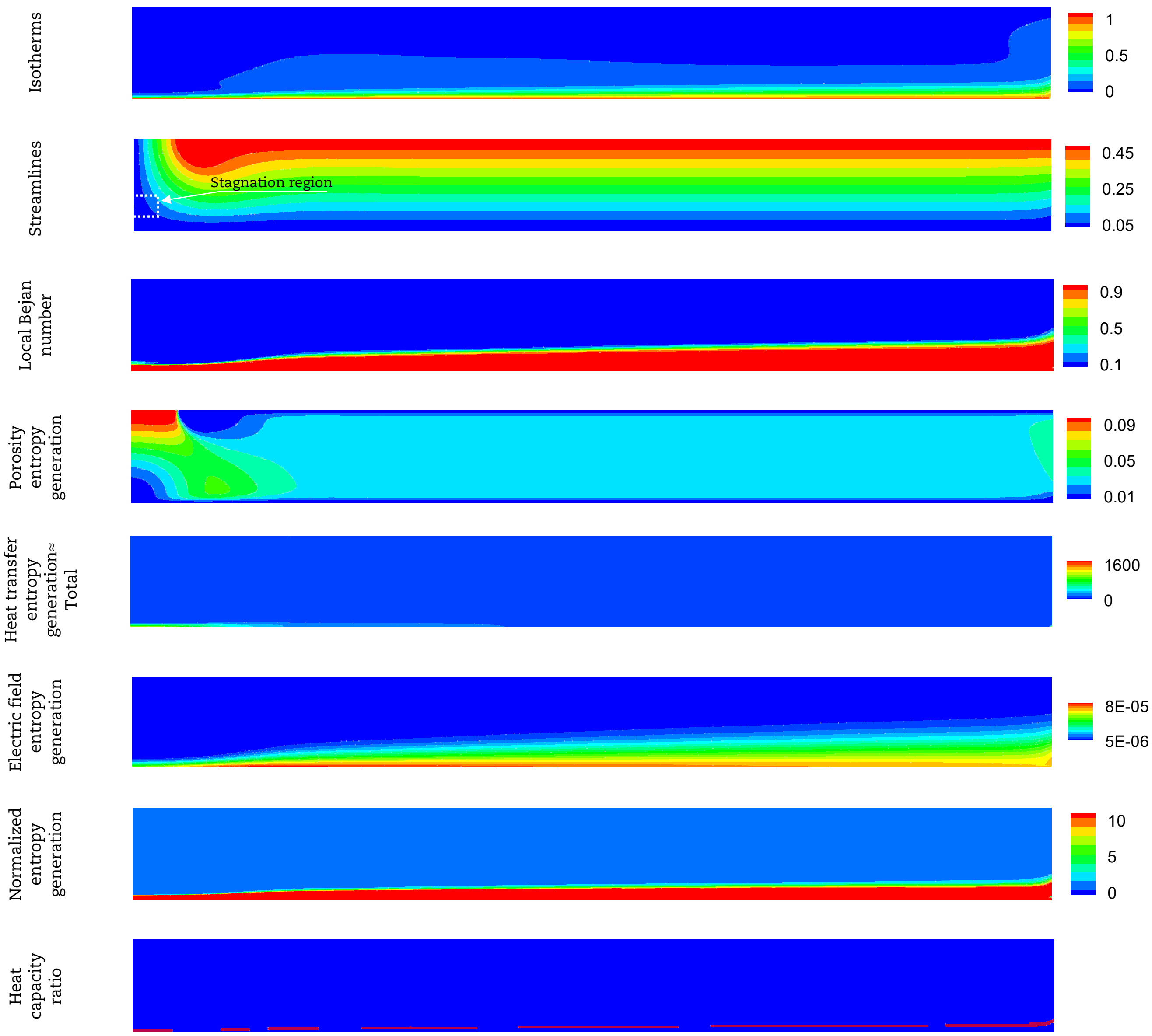

Fig. 5. The results of NEPCM-water impinging jet system at *Da* = 0.001, *Re* = 300 with EF.

For example, in the case of NEPCM-water slurry at *Re* = 100, N_{gen} decreased by about 35%, and at *Re* = 100, N_{gen} decreased by about 14% compared to water fluid alone. To assess the relative importance of $N_{gen,HT}$ across the whole medium, Be_{ave} is utilized. The Table shows the Be_{ave} reduces as the *Re* raises. For example, in the case of EMF, the values of Be_{ave} decrease from 0.39 to 0.25 (a 35.9% decrease) for NEPCM-suspension at *Da* = 0.001 when *Re* goes up from 100 to 300. This demonstrates the share of $N_{gen,HT}$ decreases by *Re*. Thus, according to the results of the Bejan number, the electromagnetic fields (meaning the combination of electric and magnetic field) exhibit a better Be in comparison with only the EF. Figures 5 and 6 illustrate the contours of isotherm, streamlines, Be_{loc}, $N_{gen,loc}$ with its components, and heat capacity ration at *Da* = 0.001, *Re* = 300 for NEPCM-water suspension in the existence of EF, and both EF and MF (*Ha* = 50), respectively. In the isotherm contour of Fig. 5, a pronounced temperature gradient is observed near the stagnation point, just beneath the inlet fluid jet. This thermal gradient becomes stronger, resulting in a thinner thermal boundary layer when subjected to the MF (Fig. 6). In other words, Both MHD and EHD effects can increase the level of turbulence in the jet. turbulence enhances convective heat transfer by continually disrupting and thinning the thermal boundary layer near the surface. However, it is noteworthy that while the heat removal ability in the stagnation zone decreases (as evident from the streamlines contour in Fig. 6), overall heat transfer increases significantly. Consequently, the application of a magnetic field that is correctly oriented reduces the width of the thermal boundary layer throughout the impingement surface while improving the flow of the imported jet fluid. By analyzing the entropy generation figures, it can be shown that the high-temperature gradients that are characteristic of the stagnation zone concentrate the isolines of entropy generation, while they are essentially nonexistent in the other regions. The Be_{ave}, which measures the contribution of heat transfer irreversibility to the N_{gen}, decreases when the MF is applied. On the other hand, there is a modest strength in the local mechanism of heat removal in the stagnation region. Put differently, the local Bejan number is near zero everywhere else and near 1 in the locations where the heat conducting mechanism is the primary heat transport method. This is because the irreversibility of viscous effects dominates the heat transfer's irreversibility. The nano-encapsulated phase-change material undergoes phase transition within its capsules in the fluid region, within the red zone that represents the *Cr* where the phase transition moves towards the cool-down region. The phase changing primarily occurs at the boundary layer of the hot plate.

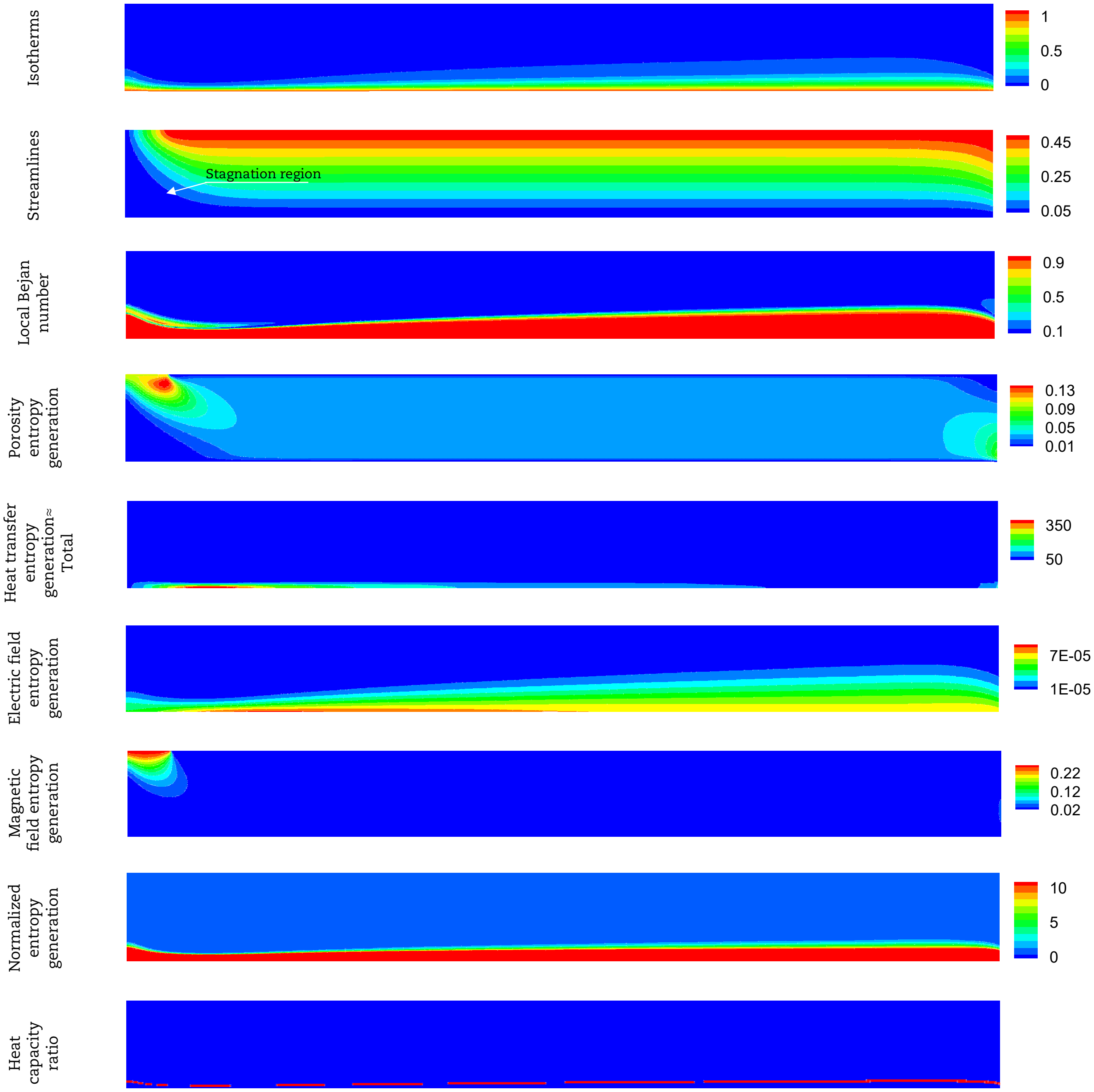

Fig. 6. The results of NEPCM-water impinging jet system at *Da* = 0.00, *Re* = 300 with EMF.

5. Conclusion

The entropy formation and heat transfer in a jet impingement system under various operating conditions such as the presence of magnetic and electric fields and the use of NEPCM-water suspension were investigated using numerical simulations in this study. The subsequent is a condensed of the primary numerical results:

- For water and NEPCM-water suspension, increasing the *Re* led to a considerable increase in the Nu_{ave} of about 67% when *Re* increased from 100 to 300. But there was also a meaningful intensification in entropy generation (N_{gen}).
- Higher heat transfer rates were caused by the presence of both electric and magnetic fields where induced Lorentz and Coulomb forces create secondary flows and cause to enhance the fluid velocity and disrupt thermal boundary layers. As seen by the Nu_{ave} values rising by about 7% for pure water and 6% for NEPCM-water suspension. In addition, entropy generation was reduced when electric and magnetic fields were combined; for NEPCM-water suspension, this resulted in a decrease of about 35% at *Re* = 100 and 14% at *Re* = 300 in N_{gen} relative to situations without fields.
- Darcy number (metal foam) improves heat transfer and circulation. The metal foam performs better in a medium without fields. For example, by setting *Da* = 0.001 in NEPCM-water at *Re* = 100, the Nu increases by around 25%. The findings show that utilizing NEPCM slurry boosts heat transfer capabilities. The best-case scenario is to use NEPCM-water in the presence of electromagnetic fields at *Re* = 300, which boosted the Nusselt number by around 6% while increasing N_{gen} by approximately 3.2%. The worst-case scenario is to use NEPCM-water at *Da* = 0.001 and *Re* = 100 without or with an electric field, where N_{gen} is approximately 65% for both scenarios.

- As the Reynolds number increased, the average Bejan number declined, showing that heat transfer irreversibility contributed less to overall entropy formation. The combination of electric and magnetic fields resulted in reduced Bejan numbers, with NEPCM-water suspension showing a 35.9% drop at Da = 0.001 and Re = 300 compared to Re = 100.
- The non-dimensional approach used for Ansys-Fluent in combination with using defined -scalars and -functions for defining complex behavior of magnetic field and electric field is completely comparable for further studies in the field of impingement jet system.

The study highlights the significant influence of Reynolds number, electric and magnetic fields, and Darcy number on heat transport effectiveness and entropy generation in jet impingement systems that use encapsulated PCM. The conclusions emphasize the importance of optimizing operating conditions, such as fluid flow parameters and external field effects, to enhance heat transfer while minimizing entropy generation in thermal systems.

Author Contributions

All authors contributed to the conceptualization and methodology of the study. M. Hashemi-Tilehnoee performed the tests simulation, E. Palomo del Barrio, and M. Sharifpur supervised the work and reviewed and edited the manuscript. All authors discussed the results, reviewed and approved the final version of the manuscript.

Acknowledgments

Not applicable.

Conflict of Interest

The authors declared no potential conflicts of interest concerning the research, authorship, and publication of this article.

Funding

The authors received no financial support for the research, authorship, and publication of this article.

Data Availability Statements

Not applicable.

References

[1] Hashemi-Tilehnoee, M., Palomo del Barrio, E., Magneto Laminar Mixed Convection and Entropy Generation Analyses of an Impinging Slot Jet of Al2O3-Water and Novec-649, *Thermal Science and Engineering Progress*, 36, 2022, 101524.

[2] Selimefendigil, F., Öztop, H. F., Pulsating Nanofluids Jet Impingement Cooling of a Heated Horizontal Surface, *International Journal of Heat and Mass Transfer*, 69, 2014, 54-65.

[3] Roy, N.C., Yesmin, F., Saha, L.K., Siddiqa, S., Electrohydrodynamics Natural Convection Flow of Nanofluids in a Rectangular Cavity Enclosed by a Corrugated Bottom Surface, *Fluid Dynamics Research*, 53(1), 2021, 015512.

[4] Roy, N.C., Saha, L.K., Siddiqa, S., Electrohydrodynamics and Thermal Radiation Effects on Natural Convection Flow in an Enclosed Domain, *International Communications in Heat and Mass Transfer*, 126, 2021, 105437.

[5] Viskanta, R., Heat Transfer to Impinging Isothermal Gas and Flame Jets, *Experimental Thermal and Fluid Science*, 6(2), 1993, 111-134.

[6] Kumar, R., Nadda, R., Kumar, S., Saboor, S., Ahamed Saleel, C., Abbas, M., Afzal, A., Linul, E., Convective Heat Transfer Enhancement Using Impingement Jets in Channels and Tubes: A Comprehensive Review, *Alexandria Engineering Journal*, 70, 2023, 349-376.

[7] Chen, L., Weigand, B., Yang, H., Shi, Y., Yang, Q., Numerical Heat Transfer Investigation of a Single Impingement Jet with Combined V-Ribs and Preliminary Optimization of V-Rib Configuration in Initial Crossflow, *International Journal of Thermal Sciences*, 197, 2024, 108799.

[8] Beitelmal, A.H., Saad, M.A., Patel, C.D., Effects of Surface Roughness on the Average Heat Transfer of an Impinging Air Jet, *International Communications in Heat and Mass Transfer*, 27(1), 2000, 1-12.

[9] Jeng, T.M., Tzeng, S.C., Experimental Study of Forced Convection in Metallic Porous Block Subject to a Confined Slot Jet, *International Journal of Thermal Sciences*, 46(12), 2007, 1242-1250.

[10] Do, K.H., Kim, T.H., Kim, S.J., Analytical and Experimental Investigations on Fluid Flow and Thermal Characteristics of a Plate-Fin Heat Sink Subject to a Uniformly Impinging Jet, *International Journal of Heat and Mass Transfer*, 53(9–10), 2010, 2318-2323.

[11] Jeng, T.M., Tzeng, S.C., Su, H.M., Hsiao, C.S., Wei, Y.C., Heat Transfer Characteristics of a Rotating Al-Foam Cylinder under the Confined/Unconfined Impinging Jet, *International Journal of Thermal Sciences*, 66, 2013, 71-81.

[12] Yakkatelli, R., Wu, Q., Fleischer, A.S., A Visualization Study of the Flow Dynamics of a Single Round Jet Impinging on Porous Media, *Experimental Thermal and Fluid Science*, 34(8), 2010, 1008-1015.

[13] Huang, X., Yang, W., Ming, T., Shen, W., Yu, X., Heat Transfer Enhancement on a Microchannel Heat Sink with Impinging Jets and Dimples, *International Journal of Heat and Mass Transfer*, 112, 2017, 113-124.

[14] Saeid, N.H., Hasan, N., Ali, M.H.B.H.M., Effect of the Metallic Foam Heat Sink Shape on the Mixed Convection Jet Impingement Cooling of a Horizontal Surface, *Journal of Porous Media*, 21(4), 2018, 295-309.

[15] Bianco, N., Iasiello, M., Mauro, G.M., Pagano, L., Multi-Objective Optimization of Finned Metal Foam Heat Sinks: Tradeoff between Heat Transfer and Pressure Drop, *Applied Thermal Engineering*, 182, 2021, 116058.

[16] Hai, T.B., Mansir, I., Alshuraiaan, B., M Abed, A., Elhosiny Ali, H., Dahari, M., Albalawi, H., Numerical Investigation on the Performance of a Solar Air Heater Using Inclined Impinging Jets on Absorber Plate with Parallel and Crossing Orientation of Nozzles, *Case Studies in Thermal Engineering*, 45, 2023, 102913.

[17] Poubeau, A., Vinay, G., Kekelia, B., Bennion, K., Numerical Simulations of High Prandtl Number Liquid Jets Impinging on a Flat Plate, *International Journal of Heat and Mass Transfer*, 205, 2023, 123889.

[18] Yousefi-Lafouraki, B., Rajabi Zargarabadi, M., Sunden, B., The Effect of Short Pin Fin Aspect Ratio on Thermal Characteristics of Intermittent Impinging Jet; An Experimental and Numerical Study, *Journal of the Taiwan Institute of Chemical Engineers*, 148, 2023, 104860.

[19] Lam, P.A.K., Prakash, K.A., Thermodynamic Investigation and Multi-Objective Optimization for Jet Impingement Cooling System with Al2O3/Water Nanofluid, *Energy Conversion and Management*, 111, 2016, 38-56.

[20] Izadi, A., Siavashi, M., Xiong, Q., Impingement Jet Hydrogen, Air and CuH2O Nanofluid Cooling of a Hot Surface Covered by Porous Media with Non-Uniform Input Jet Velocity, *International Journal of Hydrogen Energy*, 44(30), 2019, 15933–15948.

[21] Selimefendigil, F., Öztop, H.F., Jet Impingement Cooling and Optimization Study for a Partly Curved Isothermal Surface with CuO-Water Nanofluid, *International Communications in Heat and Mass Transfer*, 89, 2017, 211-218.

[22] Zhang, C.Y., Wang, T., Chen, D.H., Hong, F.J., Cheng, P., Confined Jet Array Impingement Cooling with Spent Flow Distraction Using NEPCM Slurry, *International Communications in Heat and Mass Transfer*, 77, 2016, 140-147.
[23] Mohammadpour, J., Salehi, F., Lee, A., Effective Cooling System for Solar Photovoltaic Cells Using NEPCM Impingement Jets, *Thermo*, 2(4), 2022, 383-393.
[24] Abhijith, M.S., Venkatasubbaiah, K., Numerical Investigation on Heat Transfer Performance of a Confined Slot Jet Impingement with Different MEPCM-Water Slurries Using Two-Phase Eulerian–Eulerian Model, *Thermal Science and Engineering Progress*, 33, 2022, 101315.
[25] Zhang, J.J., Yang, C.H., Jin, Z.G., Ma, S.X., Zhang, J.S., Pang, X.M., Experimental Study of Jet Impingement Heat Transfer with Microencapsulated Phase Change Material Slurry, *Applied Thermal Engineering*, 188, 2021, 116588.
[26] Mohib Ur Rehman, M., Qu, Z.G., Fu, R.P., Three-Dimensional Numerical Study of Laminar Confined Slot Jet Impingement Cooling Using Slurry of Nano-Encapsulated Phase Change Material, *Journal of Thermal Science*, 25(5), 2016, 431-439.
[27] Mohaghegh, M.R., Tasnim, S.H., Aliabadi, A.A., Mahmud, S., Jet Impingement Cooling Enhanced with Nano-Encapsulated PCM, *Energies*, 15(3), 2022, 1034.
[28] Rehman, M.M., Qu, Z.G., Fu, R.P., Xu, H.T., Numerical Study on Free-Surface Jet Impingement Cooling with Nanoencapsulated Phase-Change Material Slurry and Nanofluid, *International Journal of Heat and Mass Transfer*, 109, 2017, 312-325.
[29] Mohammadpour, J., Lee, A., Investigation of Nanoparticle Effects on Jet Impingement Heat Transfer: A Review, *Journal of Molecular Liquids*, 316, 2020, 113819.
[30] Marri, G.K., Balaji, C., Experimental and Numerical Investigations on the Effect of Porosity and PPI Gradients of Metal Foams on the Thermal Performance of a Composite Phase Change Material Heat Sink, *International Journal of Heat and Mass Transfer*, 164, 2021, 120454.
[31] Li, W.Q., Qu, Z.G., He, Y.L., Tao, W.Q., Experimental and Numerical Studies on Melting Phase Change Heat Transfer in Open-Cell Metallic Foams Filled with Paraffin, *Applied Thermal Engineering*, 37, 2012, 1-9.
[32] Nakharintr, L., Naphon, P., Magnetic Field Effect on the Enhancement of Nanofluids Heat Transfer of a Confined Jet Impingement in Mini-Channel Heat Sink, *International Journal of Heat and Mass Transfer*, 110, 2017, 753-759.
[33] Selimefendigil, F., Öztop, H.F., Al2O3-Water Nanofluid Jet Impingement Cooling with Magnetic Field, *Heat Transfer Engineering*, 41(1), 2020, 50-64.
[34] Nimmagadda, R., Haustein, H.D., Godson Asirvatham, L., Wongwises, S., Effect of Uniform/Non-Uniform Magnetic Field and Jet Impingement on the Hydrodynamic and Heat Transfer Performance of Nanofluids, *Journal of Magnetism and Magnetic Materials*, 479, 2019, 268-281.
[35] Selimefendigil, F., Oztop, H.F., Chamkha, A.J., Jet Impingement Heat Transfer of Confined Single and Double Jets with Non-Newtonian Power Law Nanofluid under the Inclined Magnetic Field Effects for a Partly Curved Heated Wall, *Sustainability*, 13(9), 2021, 5086.
[36] Hashemi-Tilehnoee, M., Seyyedi, S.M., Palomo del Barrio, E., Sharifpur, M., Analysis of Natural Convection and the Generation of Entropy within an Enclosure Filled with Nanofluid-Packed Structured Pebble Beds Subjected to an External Magnetic Field and Thermal Radiation, *Journal of Energy Storage*, 73, 2023, 109223.
[37] Hashemi-Tilehnoee, M., del Barrio, E.P., Seyyedi, S.M., Magneto-Turbulent Natural Convection and Entropy Generation Analyses in Liquid Sodium-Filled Cavity Partially Heated and Cooled from Sidewalls with Circular Blocks, *International Communications in Heat and Mass Transfer*, 134, 2022, 106053.
[38] Seyyedi, S.M., Hashemi-Tilehnoee, M., Palomo del Barrio, E., Dogonchi, A.S., Sharifpur, M., Analysis of Magneto-Natural-Convection Flow in a Semi-Annulus Enclosure Filled with a Micropolar-Nanofluid; a Computational Framework Using CVFEM and FVM, *Journal of Magnetism and Magnetic Materials*, 568, 2023, 170407.
[39] Selimefendigil, F., Öztop, H.F., Multijet Impingement Heat Transfer under the Combined Effects of Encapsulated-PCM and Inclined Magnetic Field during Nanoliquid Convection, *International Journal of Heat and Mass Transfer*, 203, 2023, 123764.
[40] Sahoo, D., Sharif, M.A.R., Mixed-Convective Cooling of an Isothermal Hot Surface by Confined Slot Jet Impingement, *Numerical Heat Transfer, Part A: Applications*, 45(9), 2004, 887-909.
[41] Izadi, A., Siavashi, M., Rasam, H., Xiong, Q., MHD Enhanced Nanofluid Mediated Heat Transfer in Porous Metal for CPU Cooling, *Applied Thermal Engineering*, 168, 2020, 114843.
[42] Seyyedi, S.M., Hashemi-Tilehnoee, M., Palomo del Barrio, E., Dogonchi, A.S., Ghadami, S.M., Sharifpur, M., Electro-Enhanced Natural Convection Analysis for an Al2O3-Water-Filled Enclosure by Considering the Effect of Thermal Radiation, *Numerical Heat Transfer, Part A: Applications*, 2023, 1-20.
[43] Hashemi-Tilehnoee, M., Dogonchi, A.S., Seyyedi, S.M., Sharifpur, M., Magneto-Fluid Dynamic and Second Law Analysis in a Hot Porous Cavity Filled by Nanofluid and Nano-Encapsulated Phase Change Material Suspension with Different Layout of Cooling Channels, *Journal of Energy Storage*, 31, 2020, 101720.
[44] Hashemi-Tilehnoee, M., Seyyedi, S.M., Palomo del Barrio, E., Sharifpur, M., Heat Transfer Intensification of NEPCM-Water Suspension Filled Heat Sink Cavity with Notches Cooling Tubes by Applying the Electric Field, *Journal of Energy Storage*, 59, 2023, 106492.
[45] Hashemi-Tilehnoee, M., Tashakor, S., Dogonchi, A.S., Seyyedi, S.M., Khaleghi, M., Entropy Generation in Concentric Annuli of 400 KV Gas-Insulated Transmission Line, *Thermal Science and Engineering Progress*, 19, 2020, 100614.

ORCID iD

Mehdi Hashemi-Tilehnoee https://orcid.org/0000-0002-0834-7805
Seyyed Masoud Seyyedi https://orcid.org/0000-0001-9490-7954
Elena Palomo del Barrio https://orcid.org/0000-0002-3846-7808
Farhad Hosseinnejad https://orcid.org/0000-0002-2835-4869
Mohsen Sharifpur https://orcid.org/0000-0003-1302-1954

How to cite this article: Hashemi-Tilehnoee M. et al., Electro-magnetic Enhanced Mixed-convection of a Confined Slot NEPCM-water Impinging Jet Equipped with Metal Foam, *J. Appl. Comput. Mech.*, 11(2), 2025, 371-381. https://doi.org/10.22055/jacm.2024.46885.4616